NASA TECHNICAL MEMORANDUM

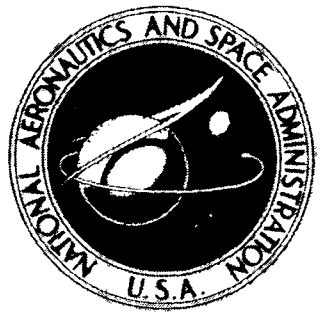

NASA TM X-2752

NASA TM X-2752

EFFECTS OF VANE-INDUCED ROTATION ON DIFFUSER FLOW DISTORTION IN AN AXISYMMETRIC MIXED-COMPRESSION INLET

by Edward T. Meleason

Lewis Research Center
Cleveland, Ohio 44135

NATIONAL AERONAUTICS AND SPACE ADMINISTRATION • WASHINGTON, D. C. • MARCH 1973

1. Report No.	2. Government Accession No.	3. Recipient's Catalog No.
NASA TM X-2752		

4. Title and Subtitle	5. Report Date
EFFECTS OF VANE-INDUCED ROTATION ON DIFFUSER FLOW DISTORTION IN AN AXISYMMETRIC MIXED-COMPRESSION INLET	March 1973
	6. Performing Organization Code
7. Author(s)	8. Performing Organization Report No.
Edward T. Meleason	E-7245
	10. Work Unit No.
9. Performing Organization Name and Address	501-24
Lewis Research Center National Aeronautics and Space Administration Cleveland, Ohio 44135	11. Contract or Grant No.
	13. Type of Report and Period Covered
12. Sponsoring Agency Name and Address	Technical Memorandum
National Aeronautics and Space Administration Washington, D.C. 20546	14. Sponsoring Agency Code

15. Supplementary Notes

16. Abstract

An investigation of vane-induced flow rotation to modify distorted steady-state total-pressure patterns in the subsonic diffuser of a supersonic mixed-compression inlet has been conducted. Radial static-pressure gradients generated by the rotation was the mechanism used to modify the total-pressure distributions. Significant redistribution of circumferential distortion patterns into more compatible radial patterns was realized, but flow problems near the duct walls reduced the general effectiveness of the technique. Total-pressure losses associated with the swirl vanes were slight. Limited turbulence data indicated that vane installation resulted in reduced turbulence levels.

17. Key Words (Suggested by Author(s))	18. Distribution Statement
Flow distortion Inlet flow Guide vanes Diffusers	Unclassified - unlimited

19. Security Classif. (of this report)	20. Security Classif. (of this page)	21. No. of Pages	22. Price*
Unclassified	Unclassified	35	$3.00

* For sale by the National Technical Information Service, Springfield, Virginia 22151

EFFECTS OF VANE-INDUCED ROTATION ON DIFFUSER FLOW DISTORTION IN AN AXISYMMETRIC MIXED-COMPRESSION INLET

by Edward T. Meleason

Lewis Research Center

SUMMARY

An investigation of flow rotation as a technique to modify distorted steady-state total pressure patterns generated by a supersonic inlet has been conducted in the Lewis 10- by 10-Foot Supersonic Wind Tunnel at Mach 2.58. Rotation was induced by thin vanes with a radial turning variation mounted in the annular diffuser of the inlet. This rotation produced radial static-pressure gradients in the subsonic diffuser flow, which acted to redistribute the total pressure patterns. Average Mach number directly ahead of the vanes varied from 0.32 to 0.41. The inlet used to generate the distortion patterns was an axisymmetric mixed-compression inlet with a design Mach number of 2.5 and 60-percent internal area contraction.

The effects of the vanes on circumferential, tip-radial, and relatively uniform distortion patterns produced by the inlet were determined at locations 0.5 and 2.0 duct diameters downstream of the vanes. It was desired to modify the circumferential and tip-radial patterns to a consistently hub-radial pattern.

Test results indicated that this method of reshaping inlet distortion patterns is potentially useful but requires further development. After passing through the vanes, the circumferential patterns developed a definite hub-radial character except in the vicinity of the outer annulus wall. Near the outer wall, static-pressure gradients sufficient to force flow redistribution were not successfully established and completely radial total pressure patterns did not develop. As a result of this same lack of flow redistribution near the outer wall, the vanes were not effective in modifying tip-radial patterns in which the lower recovery flow is concentrated in an outer ring. Losses in total-pressure recovery associated with the vanes were not large, varying from less than 0.005 for high recovery flow slighly downstream of the swirl vanes up to 0.02 for lower recovery flow 2.0 duct diameters downstream. Limited turbulence data showed that installation of the vanes resulted in reduced turbulence levels for the distorted flow patterns.

INTRODUCTION

Recent studies evaluating the tolerance of turbojet or turbofan engines to flow distortion at the compressor face have emphasized that the spatial distribution or pattern of the distortion is of paramount importance. Both circumferential and radial distortion components need to be considered. Circumferential distortion is generally more difficult for an engine to accept because of its unsymmetrical character. This type of distortion can be generated by operating the inlet at angles of attack or yaw, through boundary-layer ingestion or through some other type of flow nonuniformity entering the inlet. Pure radial distortion, on the other hand, is symmetrical and is more readily tolerated by an engine, particularly if it is anticipated in advance so that the compressor design can account for it. Of the various types of radial distortion patterns, those with the lower energy flow concentrated to the outside (tip radial) have generally proven more troublesome to turbojet engines from a compatibility standpoint than those with lower energy flow near the center (hub radial). This is due at least in part to higher blade velocities as well as secondary flow complications near the tip. Turbofan engines, however, generally have the fan lightly loaded and are tolerant of tip-radial distortion, although circumferential distortion remains a compatibility problem.

In view of these considerations, there could be some benefit from a flow mixing technique that could redistribute the troublesome circumferential and, for turbojet engines, tip-radial distortion patterns into a more easily tolerated hub-radial pattern. One technique offering such promise involves the use of turning vanes similar to inlet guide vanes but with a large radial variation in turning angle. By increasing flow velocity at the hub with respect to the tip, a radial pressure gradient can be established acting from tip to hub. This gradient would tend to draw the lower energy flow toward the hub, and, if sufficient distance were available downstream of these vanes, a hub-radial distortion pattern could be expected to develop. If this redistribution could be accomplished efficiently within a distance on the order of one duct diameter, a potential solution would be available to a number of inlet-engine compatibility problems.

Published data were not available on the effect of vanes of this type used in conjunction with highly distorted flow patterns. Accordingly, an experimental program was established at Lewis to investigate the effectiveness of this technique in an actual operating inlet situation. A high performance, axisymmetric, mixed-compression inlet was used to generate the distortion patterns.

The test was conducted in the Lewis 10- by 10-Foot Supersonic Wind Tunnel at Mach 2.58 and a Reynolds number of 3.88×10^6 based on inlet lip diameter. A variety of total-pressure distortion patterns were generated in the inlet diffuser by varying inlet angle of attack and diffuser bypass flow. These included circumferential, tip radial, and relatively uniform flow profiles. A constant area duct behind the inlet had provisions for mounting 20 thin sheet metal swirl vanes near the diffuser exit. Instrumentation rakes

were positioned in the duct downstream of the vane mounting location to measure total-pressure distributions with and without the vanes installed. These interchangeable rakes were mounted at locations either 0.5 or 2.0 duct diameters downstream of the vane trailing-edge position. Limited measurements of local flow angle and fluctuating total pressure (turbulence) were also obtained.

U.S. Customary units were used in the design of the test model and in recording and computing the experimental data. Then units were converted to the International System (SI) for use in this report.

SYMBOLS

c	vane chord, cm
f	free vortex factor, $rV\theta/(r_{tip}V\theta_{tip})$, dimensionless
H	total height of annulus, cm
h	distance from centerbody surface, cm
M	Mach number, dimensionless
P	total pressure, N/m^2
ΔP_D	$P_{D,max} - P_{D,min}$, N/m^2
p	static pressure, N/m^2
R_c	inlet capture radius, 0.2366 m
R_v	vane centerline radius of curvature, cm
r	radial distance from model centerline, cm
s	distance between vane centerlines, cm
t	vane thickness, cm
$V\theta$	tangential velocity component, dimensionless
x	axial distance from design spike tip position, cm
θ	vane outlet angle, deg
θ_l	cowl-lip-position parameter, $\tan^{-1}[1/(x/R_c)]$, dimensionless
σ	vane solidity, c/s, dimensionless

Subscripts:

D	conditions in constant area annular duct
L	local

l cowl lip

max maximum

min minimum

tip conditions at $h = h_{max}$

0 free stream

Superscript:

$-$ average

APPARATUS AND PROCEDURE

Inlet Model

The supersonic inlet used to generate distortion patterns for this investigation was an axisymmetric mixed-compression inlet with a translating centerbody to facilitate inlet start and off-design operation. At the design Mach number of 2.5, 40 percent of the supersonic flow area contraction was external, and 60 percent was internal. Detailed descriptions of the inlet design and component hardware are presented in reference 1. Although the inlet was designed for Mach 2.5 operation, the test was conducted at Mach 2.58 since higher angles of attack with resultingly more severe circumferential distortion patterns could be obtained at the higher Mach number.

The inlet-nacelle installation is shown in figures 1(a) and (b). The basic inlet configuration (fig. 1(c)) is identical to the model tested in reference 1. Boundary-layer bleed capability was available through porous regions on the centerbody and cowl in the supersonic diffuser and throat region of the inlet. Vortex generators were installed on the centerbody in the subsonic diffuser to prevent separation of flow from the centerbody in the bypass region when large overboard bypass flows were discharged. The overboard bypass was used to modify flow distortion patterns produced by the inlet. The centerbody spike is shown in the Mach 2.5 design position in figure 1(c). At the test Mach number of 2.58 the centerbody was translated forward 0.50 centimeter from the design position to allow shock-on-lip operation. This spike position corresponded to a value of $\theta_l \doteq 26.23^{\circ}$, where θ_l is the angle between the spike tip and the cowl lip.

Model hardware downstream of the inlet is shown in figure 1(d). The cold-pipe configuration provides a long constant-area extension of the inlet diffuser with provisions for mounting swirl vanes and instrumentation surveys. When installed, the vanes leading edges were located at $x = 200.66$ with the trailing edges about 5.0 centimeters further downstream. There were two alternate instrumentation survey planes located approximately 0.5 and 2.0 duct diameters downstream of the vane trailing edges at stations 1

and 3, respectively. The remotely actuated choked-exit plug was used to vary inlet corrected weight flow.

The inlet normal hole bleed configuration used throughout the test is shown in figure 2. This bleed pattern is identical to configuration I of reference 1 and configuration A of reference 2. All bleed is ahead of the geometric throat. At the test Mach number of 2.58, the total bleed removed by this system was about 2.7 percent of the capture mass flow, with 1.2 percent from the cowl and 1.5 percent from the centerbody.

During the course of the test program, the inlet was used to generate three distinct types of total-pressure distortion patterns in the cold pipe annulus, specifically circumferential, tip-radial, and relatively uniform distributions. Circumferential patterns were achieved by operating the inlet at 4.7° angle of attack, very close to the limiting angle above which the inlet would unstart. For tip-radial patterns the inlet was positioned at a 0° angle of attack. The relatively small amount of cowl bleed plus the absence of vortex generators on the cowl surface contributed to the development of a tip-radial pattern. Relatively uniform patterns were generated, with the inlet again at 0°, by using the overboard bypass valves in the diffuser to remove about 11 percent of the capture mass flow. Since the bypass design removes flow from the vicinity of the cowl surface, this had the effect of modifying the tip-radial patterns to distributions that were relatively uniform.

Swirl Vanes

The 20 swirl vanes (shown installed in fig. 3(a)) were fabricated from thin stainless steel sheet and comprised circular arc sections with the amount of flow turning increasing from the tip inward along the vane. Assuming uniform approach conditions, the absolute velocity would then also increase toward the hub, creating a static-pressure gradient acting from the outer to the inner wall. It was anticipated that this gradient would draw the lower energy flow toward the inner (hub) wall.

Vane geometry is described in figure 3(b) and tabulated in table I. The vane design was developed with the aid of a computer routine that calculated flow continuity and radial equilibrium conditions. Input variables included the number of vanes, vane thickness, approach flow conditions, annulus geometry, and outflow angle at the vane tip which was set at 30°. In addition, assumptions were required on the radial variation of tangential velocity $V\theta$ and the radial distribution of vane solidity $\sigma = c/s$.

A continuously increasing tangential velocity from outer to inner wall is required to generate the desired static-pressure gradient and satisfy radial equilibrium conditions. If the tangential velocity is allowed to vary inversely with radius, the resultant flow is a free vortex with the free vortex factor $f = rV\theta/r_{tip}V\theta_{tip}$ everywhere equal to 1.0. An

initially high tangential velocity is desirable near the outer wall to produce a large absolute velocity and develop a sizeable pressure gradient in this area as the velocity increases. As velocity continuously increases toward the hub, difficulties can be encountered when the absolute velocities near the hub approach sonic speed. Therefore, in practice it is difficult to maintain a free vortex (i.e., $rV\theta$ = constant) for annular ducts with hub-tip ratios less than 0.5. For vane design purposes, the free vortex factor was assumed to decrease linearly from 1.0 at the tip to 0.72 at the hub, and the maximum absolute velocity was not permitted to exceed Mach 0.9 for an approach Mach number of 0.4.

Solidity distribution was based on generally accepted design practices for annular cascade and guide vanes. A solidity variation from 1.2 at the tip to 2.0 at the hub was assumed.

From these inputs the complete blade geometry and resultant flow could be calculated. Iterations proceeded toward the design goal of a vane configuration such that the maximum local induced velocity was near Mach 0.9 for an approach Mach number of 0.4. Mach 0.4 was near the maximum Mach number anticipated in the constant area aft diffuser section of the inlet at a free-stream Mach number of 2.58. With no overboard bypass flow, the minimum Mach number in this section would be about 0.345.

The theoretical performance of the final vane design, with uniform approach Mach numbers of 0.345 and 0.40, is presented in figure 4. The induced radial variations in local Mach number, static pressure, and flow angle are shown. Note that most of the theoretical variation in these properties occurs in the inner part of the annulus. The end points for the computer calculations were set at locations corresponding to 1 percent of the total annulus area away from the walls to get outside most of the boundary layer. However, the curvature at these points was continued to the surface so that rotation was induced in the boundary-layer flow also. This situation may have contributed to the development of the exceptionally low local total pressures near the hub that were observed in some cases with the vanes installed.

Model Instrumentation

The inlet static-pressure instrumentation described in references 1 and 2 was included for the present test but was used only to establish inlet operating conditions and to verify their repeatibility. The array of six total-pressure rakes normally located at 174.98 centimeters from the spike tip for measurement of inlet recovery and distortion (refs. 1 and 2) were removed to eliminate any interference they might have on the flow surveys further downstream. These downstream flow measurements in the constant area annular duct were accomplished using the rake arrangement shown in figure 5(a). There

were eight probes on each rake, including a single dynamic total-pressure probe located near the middle of the annulus. Five of the rakes otherwise consisted of steady-state total-pressure probes, and the sixth was made up of probes designed to measure flow angularity in the circumferential direction. The spacing of these seven-probe groups consisted of five equal-area-weighted positions with an additional probe added on either side of the equal-area-weighted probe nearest the hub in positions corresponding to a 15-tube area-weighted rake. The six-rake array was installed at either of two stations, which were located 20.40 and 81.36 centimeters downstream of the vane trailing edges and are referred to as stations 1 and 3, respectively. As mentioned previously, these locations were approximately 0.5 and 2.0 duct diameters downstream of the vane trailing edges. The arrangement of 12 static pressure taps (fig. 5(a)) was located at each of the two rake stations and also at station 2, midway between them.

The various types of probes were all designed for high angular tolerance and maintained their accuracy out to relative flow angles of 30° to 35°. Details of the probes and their accuracies are described below. For measurements without the swirl vanes installed, the rakes were mounted with the probe axes parallel to the longitudinal axis of the model. With the vanes installed, the theoretical flow angles varied between 30° and 55° and the probes were mounted with their axes at 45° to the model longitudinal axis (fig. 5(b)). This arrangement reduced the local flow angles relative to the probes to within the accepted accuracy limits.

Details of the steady-state total-pressure probe design are shown in figure 5(c). As reported in reference 3, this type of vented shield configuration is capable to considerably larger flow angle tolerance than nonshielded tubes. In calibration tests at Mach 0.4 and with the particular probe design shown in figure 5(c), the variation of measured total pressure with local flow angle was flat out to $\pm 35^{\circ}$, and there was still less than 1-percent deviation at $\pm 40^{\circ}$. The steady-state flow angularity probe (fig. 5(d)) was designed at Lewis and is described in reference 4. This type of probe utilizes calibrated differential pressures to define the local flow angle relative to the probe. Measurement accuracy has been established as within $\pm 0.5^{\circ}$ for flow angles up to $\pm 30^{\circ}$. The total pressure measured by the middle tube of these probes was calibrated as a function of local flow angle, corrected, and used as part of the measured total-pressure distribution. The dynamic total-pressure probe design (fig. 5(e)) was a shielded configuration incorporating a 0.318-centimeter-diameter Kulite transducer. The transducer face was protected from particle damage by a vented cap. In development tests of this design, the variation of transducer signal with flow angle was flat out to 30°.

The total pressure recoveries and distortions referred to in other sections of this report were obtained by using all seven tubes in each rake. In addition to being area-weighted, the individual total-pressure probes were also mass-flow-weighted when the vanes were installed, based on the theoretical radial mass-flow variation. The effect of this mass flow weighting on the total pressure average was quite small, on the order of

0.2 percent. However, all total-pressure recovery data presented for cases where the vanes are installed include the mass flow weighting correction. The total-pressure fluctuation parameter presented in the data figures is an average of the rms measurements from the six transducers.

No attempt was made to measure mass flow through the duct with the choked exit plug. The extensive hardware in the cold-pipe upstream of the plug and the large angular flow components induced by the vanes made mass-flow measurements questionable. Instead, the average static-pressure ratio at the normal inlet performance measurement station (174.98 cm from the spike tip) was correlated with duct corrected weight flow during a previous test of this same inlet configuration. This correlation was then used to calculate duct corrected weight flow for identical inlet conditions during the present test.

RESULTS AND DISCUSSION

The results of the investigation will be discussed in three parts: first, the effect of the vanes on diffuser flow with circumferential total pressure distortion patterns; second, the effect on flow with tip-radial patterns; and third, the effect on flow with relatively uniform patterns and low distortion levels.

Effect on Flow with Circumferential Distortion

Circumferential distortion patterns were generated in the inlet diffuser duct by operating the model at an angle of attack of 4.7°. At this condition, total-pressure distributions with and without the swirl vanes installed are shown in figure 6. Stations 1 and 3 are approximately 0.50 and 2.00 duct diameters downstream of the vane trailing edges, respectively. In figure 6(a) flow patterns are presented at the minimum corrected weight flow condition, just before inlet unstart. As can be seen, the vanes produced considerable modification of the original highly circumferential pattern, but the desired hub-radial pattern was not fully achieved. Increased distance allowed the progressive transfer of high-recovery flow to the outside and low-recovery flow to the inside. However, a large segment of the low-recovery flow remained close to the outer wall, and it was only away from the wall that a highly radial pattern became established.

In figure 6(b) the effect of the vanes on a different circumferential flow pattern is presented. This pattern was achieved by opening the exit plug, which resulted in increased corrected weight flow with the terminal shock moving downstream of the inlet throat (supercritical operation). As in the previous case, the vanes resulted in considerable redistribution of the flow and at station 3 a radial pattern was established away from the vicinity of the outer wall. Near the outer wall, the patterns were still highly

circumferential in character even at station 3. The average approach Mach numbers for these two conditions were approximately 0.35 for the minimum corrected weight flow case and 0.38 for the supercritical case.

Since it was impractical to duplicate inlet operating conditions exactly, the various flow patterns compared in figures 6(a) and (b) represent closely similar but not necessarily equivalent corrected weight flow conditions. For this reason the individual values of total-pressure recovery and distortion presented in figures 6(a) and (b) were included to indicate trends rather than exact comparisons. In figure 7 diffuser flow properties with and without vanes at the two measuring stations are plotted against corrected weight flow, allowing direct comparisons to be made. A small but definite loss in total-pressure recovery associated with the vanes can be seen, and this loss increases with downstream distance. At station 1, 0.5 duct diameter downstream of the vanes, a consistent recovery loss of about 0.005 is indicated. Two diameters downstream at station 3, the recovery loss varies from about 0.007 at the high-recovery levels to more than 0.02 at lower recoveries. The variation of total-pressure distortion with and without the vanes installed can be seen in the middle group of curves in figure 7. Without vanes, the attenuation of distortion with distance can be seen. With the vanes installed, total-pressure distortion becomes slightly higher at station 1 and markedly higher at station 3. A comparison of the station 3 flow patterns with and without vanes in figure 6(b) indicates where this increased distortion is coming from. A ring of low recovery flow encircles the hub with the vanes installed, and without the vanes a recovery region of this low magnitude is not present anywhere in the pattern. These exceptionally low total pressures near the hub at the downstream station result from boundary-layer thickening as the lower recovery flow is progressively transferred to the vicinity of the hub. The effect of the vanes on rms total-pressure fluctuation is shown in the lower set of curves of figure 7. As mentioned previously, this parameter is based on an average of six measurements at a single radial location near the center of the duct. Without the vanes installed a rather surprising increase in rms level is seen in moving downstream from station 1 to station 3. A possible explanation is that the pressure fluctuations at station 3 are being influenced by vortex shedding from the cylindrical support struts slightly downstream of this station. As seen in figure 1(d) the measuring station is about 15 centimeters ahead of the struts, which were designed with circular cross sections in view of the wide range of local flow angles they would encounter. The pressure fluctuations were not recorded for subsequent frequency analysis, so that the influence of any vortex shedding on the turbulence measurements can not be substantiated. Of greater interest is the general marked reduction in average rms level that occurs at both measuring stations with the vanes installed.

Some insight into the failure of the vanes to completely redistribute the circumferential flow patterns can be gained by examining the measurements of local flow angle in

figure 8. Although these angles were measured at the single 90° circumferential position, it is felt that the trends exhibited by the data would not be a strong function of circumferential location but would generally apply throughout the flow field. If uniform approach conditions are assumed, then radial angle variation is related directly to local static pressure, with the hub-directed pressure gradient increasing as flow turning increases. In the theoretical variations shown in figure 4, the flow angle continuously increases from the tip to the hub, resulting in a continuously decreasing static pressure from the outer to the inner wall. This pressure gradient should then redistribute the flow by drawing the lower energy flow toward the hub. However, near the outer wall the local gradient in theoretical static pressure is quite small. In figure 8 the measured flow angles near the outer wall are generally less than and of opposite slope to their theoretical distribution. This result indicates that the actual static-pressure gradient in this region is quite likely not as great as the already small theoretical gradient. In any event the flow patterns of figure 6 indicate that the existing static-pressure gradient near the outer wall is not sufficient to overcome the axial momentum of the lower recovery flow and move it from the wall. This marked deviation from the theoretical flow angle distribution in the outer part of the duct, with low measured angles and usually a reverse slope near the outer wall, was present for all of the various distortion patterns tested. The cause of this deviation is not apparent from the data available. Possibly the vanes are spaced too widely in this region to produce full turning, or perhaps secondary flow effects such as induced vorticity from the vane tips are involved. Near the inner (hub) wall the slope of the flow angle distribution also deviates from the theoretical. This local deviation occurred only with the highly distorted circumferential patterns; for the other patterns, which will be subsequently discussed, the measured angle variation near the hub wall approximated the theoretical prediction. The extreme variation of figure 8(b) for the station 3 point near the hub is caused by an exceptionally low local total pressure at that point, which probably represents boundary-layer immersion. Away from the walls, the slope of the actual flow angle variation is generally steeper than the theoretical variation. It is of interest to note that when the vanes were not installed, local flow angles were within a few degrees of zero for these highly circumferential flow patterns.

In figure 9 wall static pressures are shown at the three measuring stations with and without the vanes installed. The low hub pressures induced by the vanes dissipate quickly with distance, so that the overall pressure differential between the outer and inner walls becomes considerably reduced from the theoretical value. However, this is strictly a wall effect and in the middle of the duct the flow angle measurements of figure 8 indicate that the gradients did not dissipate appreciably with distance.

Effect on Flow With Tip-Radial Distortion

Tip-radial distortion patterns were generated by operating the inlet at 0° angle-of-attack. The small amount of cowl bleed plus the absence of vortex generators on the cowl surface contributed to the development of the tip-radial pattern. Total pressure distributions with and without the vanes installed at stations 1 and 3 are shown in figure 10.

In figure 10(a) the results are for the minimum corrected weight flow condition, just before inlet unstart. It can be seen that the vanes were not successful in breaking up the ring of lower recovery flow around the outer wall. The main effect of the vanes was the development of an inner ring of lower recovery flow at the centerbody. This inner ring probably represents local losses at the hub induced by the vanes rather than actual flow transfer from the vicinity of the outer wall, since the outer ring of lower energy flow was not diminished in extent.

In figure 10(b) flow patterns are shown with and without vanes for a different, somewhat more severe tip-radial distribution generated by operating the inlet supercritically. At this slightly higher average duct Mach number (0.37 against 0.345), essentially the same results were obtained. However, at station 3 with the vanes installed there is evidence of the low energy outer ring beginning to break up. Some unusually low recovery flow is present at the centerbody but outside this small ring the distortion level is only about 0.04.

The variation of diffuser flow properties with and without the vanes is presented in figure 11. Again, a small but definite recovery loss is associated with the vanes, varying from about 0.002 at station 1 for high total pressure recovery conditions to more than 0.02 at station 3 with lower recoveries. The variation in the steady-state distortion parameter is similar to that encountered with the circumferential distortion patterns. At station 1, 0.5 duct diameters downstream, the vanes have little effect on distortion. Further downstream at station 3 the distortion increases by as much as 100 percent when the vanes are installed. This distortion increase at station 3 becomes greater as corrected weight flow increases (higher duct Mach numbers) and is again attributed to the development of unusually low recovery flow at the hub. As in the circumferential distortion case, the vanes resulted in marked reductions in total-pressure fluctuation level at both stations 1 and 3.

Flow angle measurements at the 90° circumferential position shown in figure 12 again indicate the failure of the vanes to establish the desired slope of the flow angle variation at the outer wall. As a consequence, the hub-directed static pressure gradient at the tip was probably reduced from its theoretical level. In any event the gradient was not sufficient to redistribute the flow pattern, since the ring of lower recovery flow at the outer wall remained there as previously indicated. Near the inner wall the measured

flow angles are close to theoretical values and the variation is much better behaved than in the circumferential case shown in figure 8. Very little dissipation of flow angle with distance takes place in going from station 1 to station 3.

Effect on Relatively Uniform Flow

Relatively uniform flow patterns were generated by operating the inlet at zero angle-of-attack and bypassing about 11 percent of the capture mass flow. This removed most of the lower recovery flow from near the outer diffuser wall, modifying the tip-radial patterns just discussed into relatively flat total-pressure profiles. Flow patterns with and without the vanes installed are shown for the minimum corrected weight flow condition, just before inlet unstart, in figure 13(a). Because of the bypass flow removal, the average duct Mach number at this condition was reduced to about 0.32. As indicated in figure 13(a), the low distortion pattern was basically unchanged by the vane installation. When the inlet was operated supercritically in this configuration, a modified tip-radial pattern was generated, and the influence of the vanes on this pattern is shown in figure 13(b). As with the previous tip-radial distributions, the vanes had little effect other than the buildup of an inner ring of lower recovery flow around the centerbody at station 3.

The effect of the vanes on diffuser flow properties with relatively uniform flow patterns is shown in figure 14. The loss in total pressure recovery associated with the vanes is about 0.005 at high-recovery low-distortion conditions and increases to more than 0.01 as the inlet is operated supercritically and corrected weight flow increases. An effect of distance is again seen, with the downstream station showing more of a loss. The total-pressure distortion data displays the same trend previously observed for the other patterns. The steady-state distortion parameter showed little change with vane installation at station 1, but at station 3 the vanes produced a marked rise in distortion, which increased with corrected weight flow. As with the other patterns, this increased distortion was associated with the development of unusually low recovery flow near the hub wall. There was little effect of the vanes on the total-pressure fluctuation parameter except at station 3, where the extremely low turbulence levels at low corrected weight flows were increased by vane installation. Of interest is the behavior of the total-pressure fluctuation parameter with duct length for the case where the vanes are not installed. Initially, at low values of corrected weight flow and hence low duct Mach numbers, the turbulence levels are slightly lower at station 3 than at station 1 further upstream. This agrees with conventional flow behavior where turbulence dissipates with increasing duct length. As corrected weight flow increases, the turbulence level at station 3 remains below or near the level at station 1 until a sharp increase is noted near a corrected weight flow of 17 kilograms per second. Possibly some disturbance from the

circular support struts such as the previously mentioned vortex shedding begins to influence the transducer measurements near this point.

The measured flow angle variations with and without the vanes installed for the relatively uniform flow profiles are shown in figure 15. With vanes, the now familiar deviation from the theoretical slope near the outer wall is once again encountered. Thus, even with low-distortion high-recovery flow near the outer wall, the vanes were unsuccessful in establishing the desired angular variation. As with the tip-radial pattern, the flow-angle variation near the hub wall is close to the theoretical slope and is well established.

CONCLUDING REMARKS

Although some aspects of the experimental results are encouraging, the observed lack of significant radial flow redistribution in the outer part of the annulus restricts the usefulness of this particular vane design. Flow-angle measurements for the various distortion patterns show a consistent deviation from theoretical values in this outer annulus region, indicating some basic flow problem is reducing vane effectiveness. As previously mentioned, the most likely explanations are considered to be either a secondary flow effect influencing flow turning near the outer wall or the vanes may be spaced too widely in this region to turn the flow effectively. Possibly a combination of these influences is at work. If secondary flow effects are the predominant problem, it would seem that vane performance could be improved by modifying vane curvature near the outer wall to compensate for these effects. On the other hand, vane spacing could be reduced by incorporating stub vanes at the outer wall extending only partially across the annulus. It is felt that improved flow redistributions could be realized through examining the effects of vane modifications along these lines.

SUMMARY OF RESULTS

Thin vanes with a radial turning variation were investigated as a flow redistribution device to modify steady-state distortion patterns in the subsonic diffuser of a supersonic mixed-compression inlet. The effects of the vanes on circumferential, tip-radial, and relatively uniform total pressure distortion patterns produced by the inlet were determined at locations 0.5 and 2.0 duct diameters downstream of the vanes. It was desired to modify the circumferential and tip-radial patterns to a hub-radial pattern. The test was conducted in the Lewis 10- by 10-Foot Supersonic Wind Tunnel at Mach 2.58 with the following results:

(1) Significant modification of circumferential distortion patterns was achieved. However, the effectiveness of flow redistribution was limited by the failure of the vanes to establish a strong enough hub-directed static-pressure gradient near the outer annulus wall. Vane secondary flow effects possibly contributed to the problem. As a result, low recovery flow near the outer wall tended to stay there. Away from the outer wall, a strong gradient was established toward the hub, and the circumferential flow patterns developed a definite hub-radial character.

(2) The tip-radial patterns retained low energy flow near the outer wall after passing through the vanes, again because of the failure of the vanes to establish a sufficient pressure gradient in this area. There was some transfer of low energy flow to the hub indicated, but most of it remained at the outer wall.

(3) The effect of the vanes on high recovery flow with a flat, low-distortion profile was small.

(4) Total-pressure recovery losses, associated with the swirl vanes, varied from less than 0.005 for high recovery flow slightly downstream of the vanes up to 0.02 for lower recovery flow 2.0 duct diameters downstream. The losses were of these magnitudes for each of the distortion patterns tested.

(5) Steady-state distortion values were basically unchanged by the vanes at the forward flow survey station, 0.5 duct diameters downstream of the vanes, for all three distortion patterns. At 2.0 diameters downstream, the distortion was usually significantly higher with the vanes installed. In this case, the higher distortions are due to exceptionally low local total pressure near the hub, probably resulting from boundary-layer thickening.

(6) Limited turbulence data showed that installation of the swirl vanes resulted in significantly reduced turbulence levels for the circumferential and tip-radial distortion patterns.

Lewis Research Center,
National Aeronautics and Space Administration,
Cleveland, Ohio, December 4, 1972,
501-24.

REFERENCES

1. Cubbison, Robert W.; Meleason, Edward T.; and Johnson, David F.: Performance Characteristics from Mach 2.58 to 1.98 of an Axisymmetric Mixed-Compression Inlet System with 60-Percent Internal Contraction. NASA TM X-1739, 1969.

2. Cubbison, Robert W.; Meleason, Edward T.; and Johnson, David F.: Effect of Porous Bleed in a High-Performance Axisymmetric, Mixed-Compression Inlet at Mach 2.50. NASA TM X-1692, 1968.

3. Gracey, William: Wind-Tunnel Investigation of a Number of Total-Pressure Tubes at High Angles of Attack. Subsonic, Transonic, and Supersonic Speeds. NACA Rep. 1303, 1957.

4. Dudzinski, Thomas J.; and Krause, Lloyd N.: Flow-Direction Measurement with Fixed-Position Probes. NASA TM X-1904, 1969.

TABLE I. - VANE SPECIFICATIONS

Radius measured from centerline, r, cm	Vane spacing, s, cm	Vane chord, c, cm	Outlet vane angle, θ, deg	Vane radius of curvature, R_v, cm
[a]5.664	-----	3.764	48.62	4.572
5.992	1.882	3.764	48.62	4.572
7.130	2.240	4.074	45.95	5.217
8.595	2.700	4.470	42.50	6.167
10.061	3.160	4.869	39.53	7.198
11.527	3.622	5.265	36.90	8.319
12.992	4.082	5.664	34.68	9.50
14.458	4.542	6.060	32.80	10.734
15.923	5.004	6.459	31.19	12.012
17.389	5.464	6.855	29.96	13.261
18.854	5.923	7.254	29.08	14.445
20.226	6.355	7.625	28.62	15.425
[b]20.523	-----	7.625	28.62	15.425

[a]Inner annulus (hub).

[b]Outer annulus (tip).

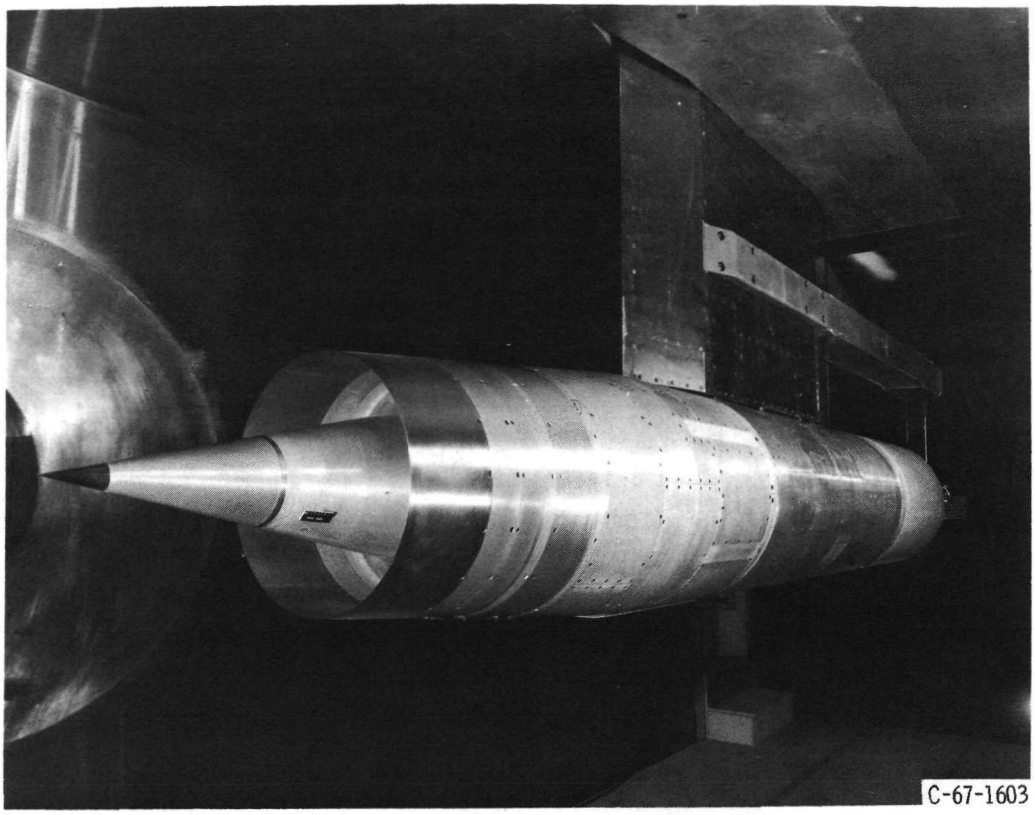

(a) Model installed in the 10- by 10-foot supersonic wind tunnel.

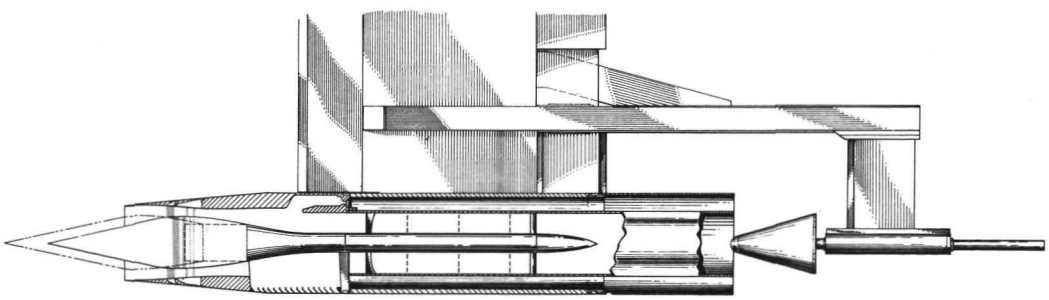

(b) Nacelle cutaway.

Figure 1. - Model configuration.

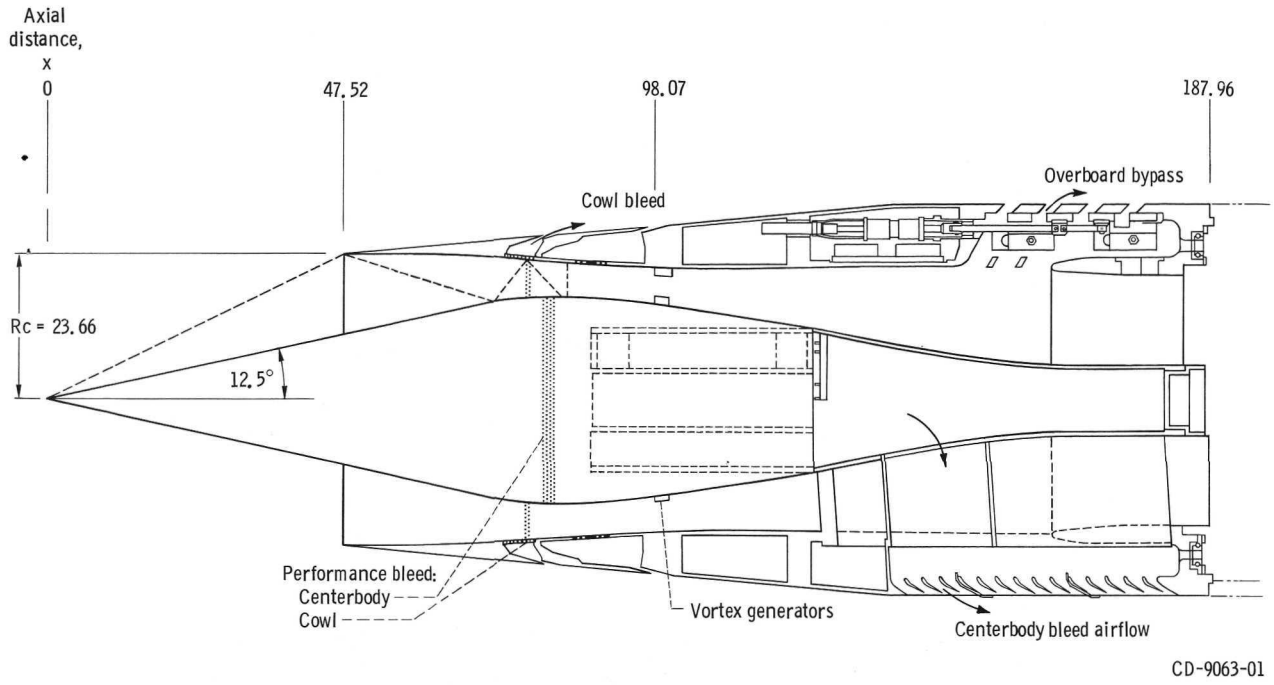

(c) Inlet details (dimensions are in cm).

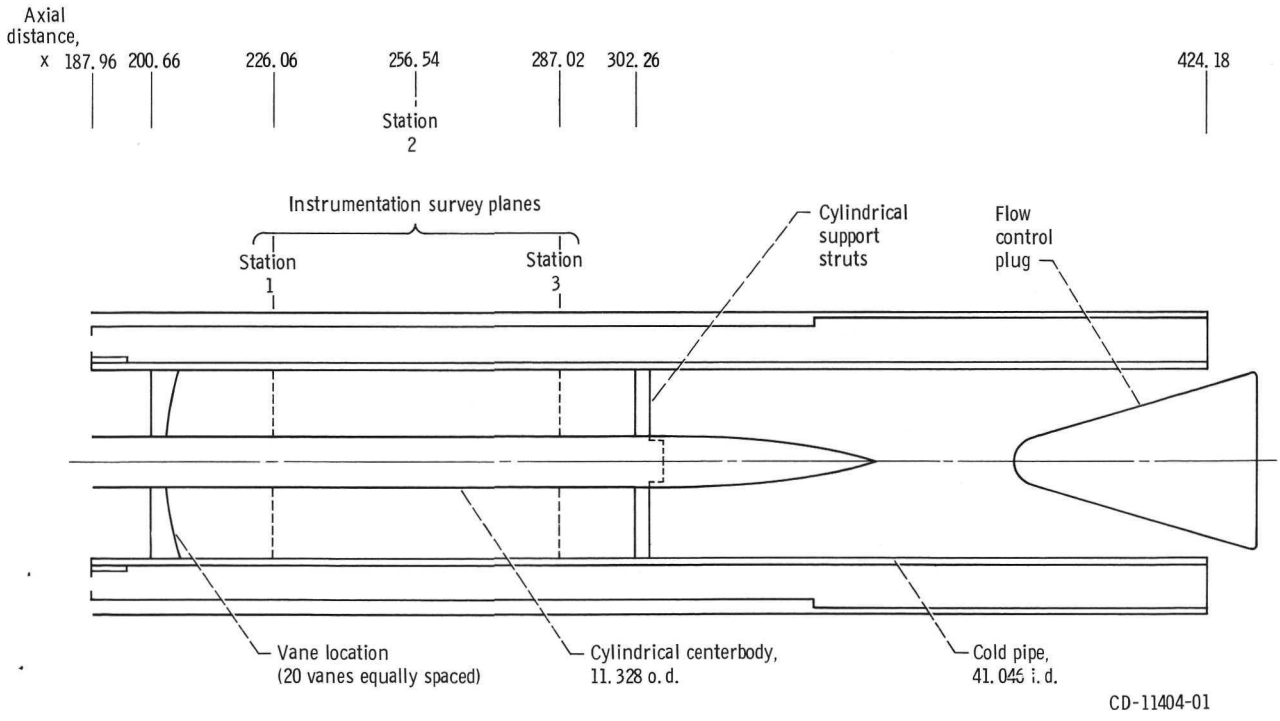

(d) Cold pipe details (dimensions are in cm).

Figure 1. - Concluded.

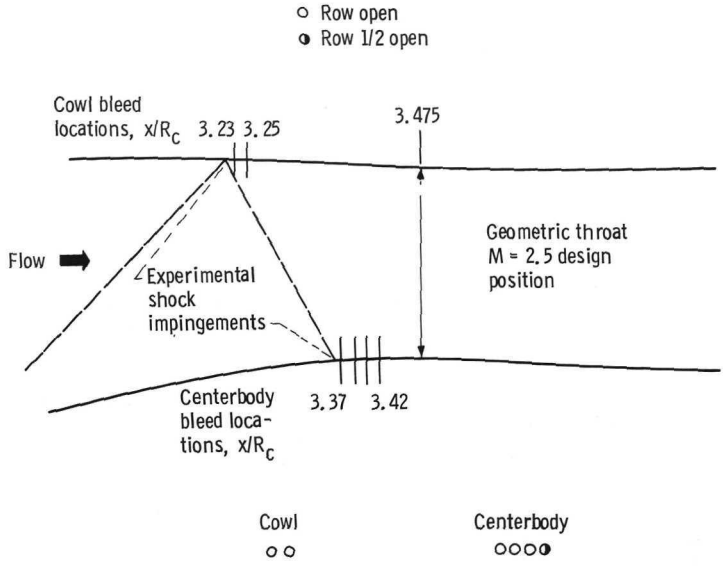

Figure 2. - Inlet normal hole bleed configuration.

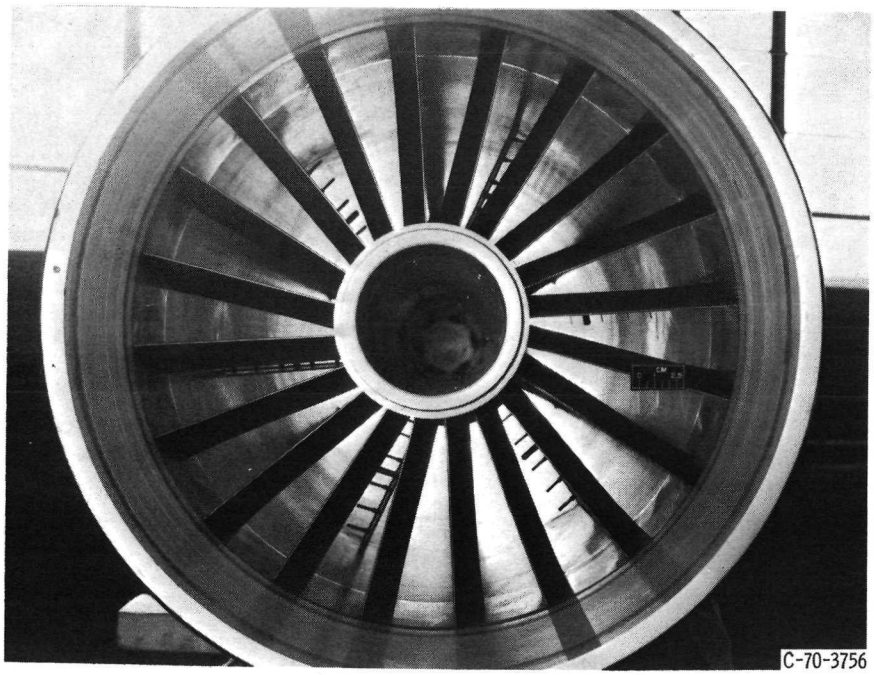

(a) Vanes installed in cold pipe, looking downstream.

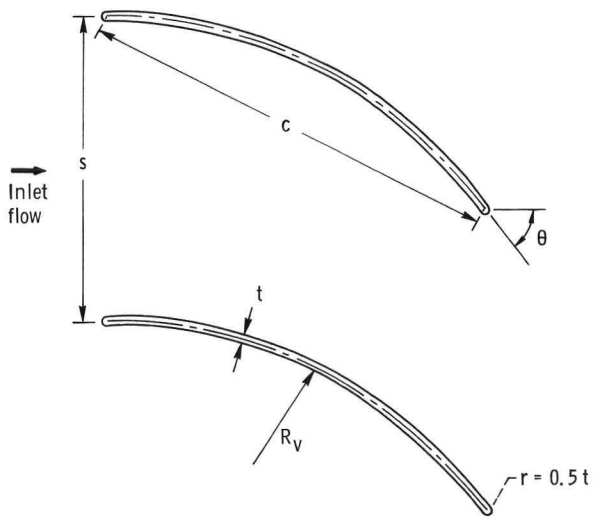

(b) Vane nomenclature. Twenty vanes equally spaced; circular arc vane sections; vanes formed from 0.157-centimeter (0.062-in.) stainless-steel sheet; initial vane angle, 0^{o}; vane curvature counterclockwise (viewed from upstream).

Figure 3. - Swirl vane configuration.

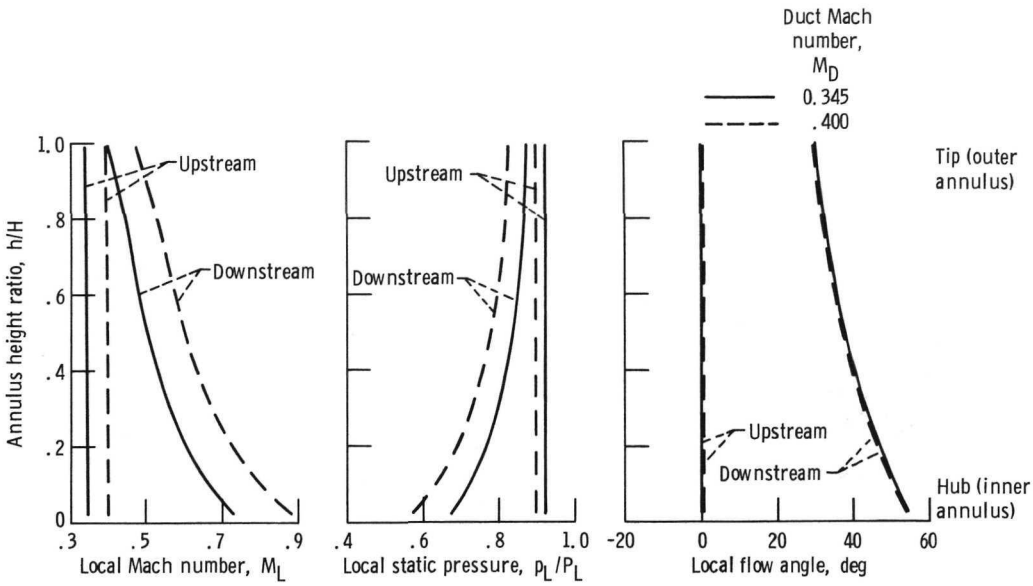

Figure 4. - Theoretical performance of swirl vanes mounted in annular duct.

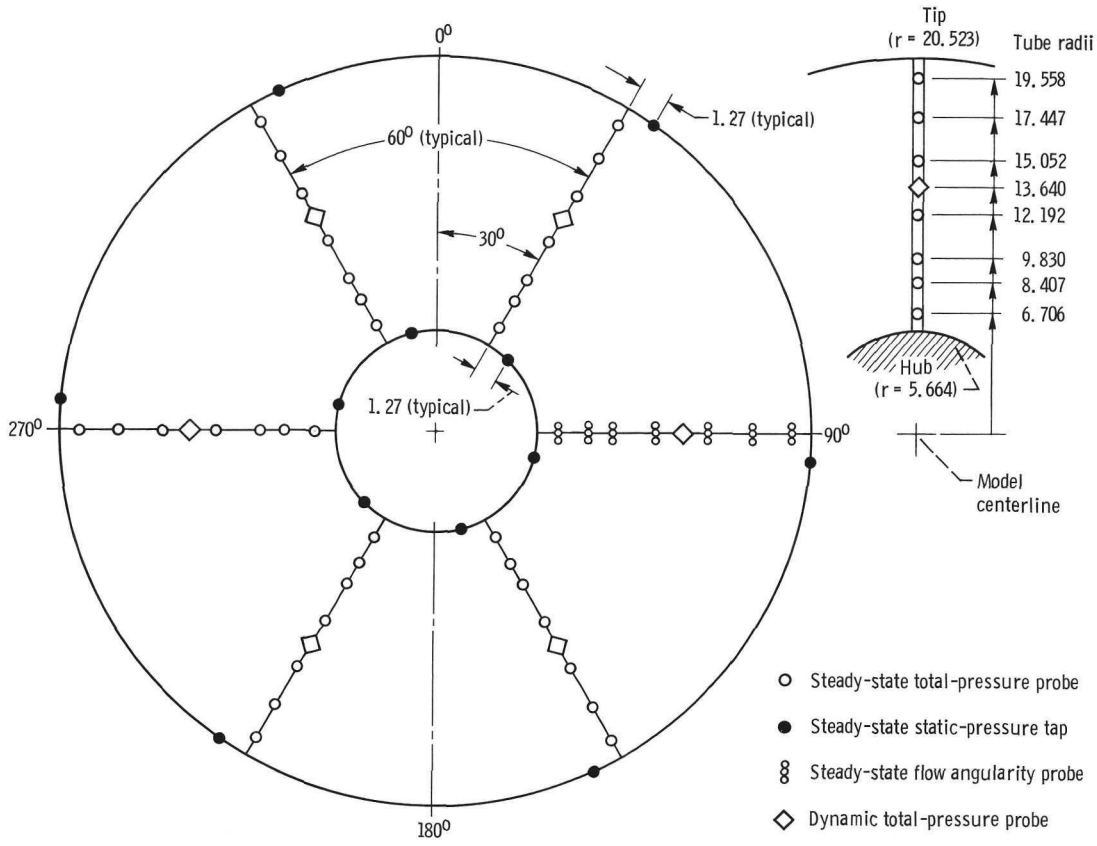

(a) General arrangement looking downstream. (All linear dimensions are in cm.)

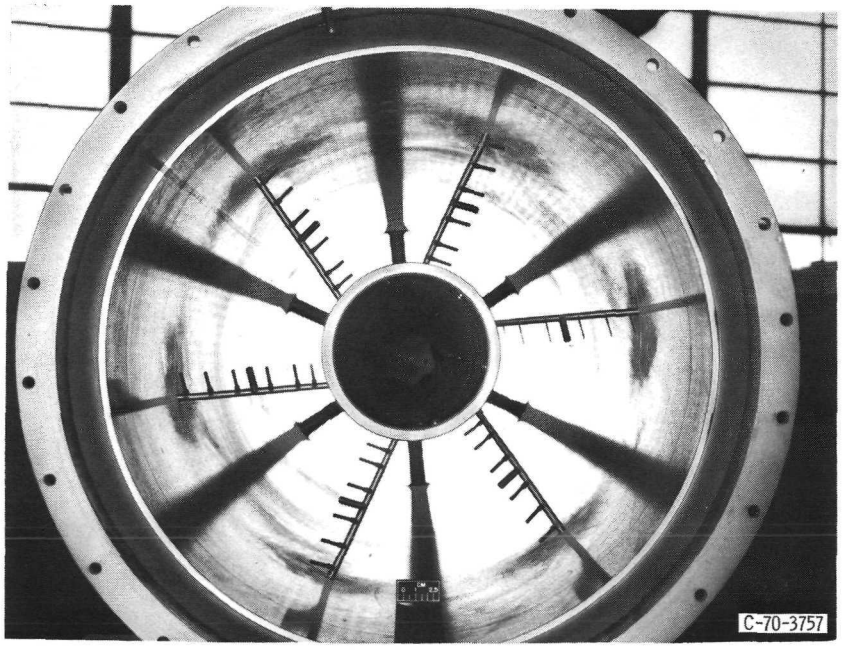

(b) Rake installation looking downstream. Rakes at 45°.

Figure 5. - Instrumentation at cold pipe survey station.

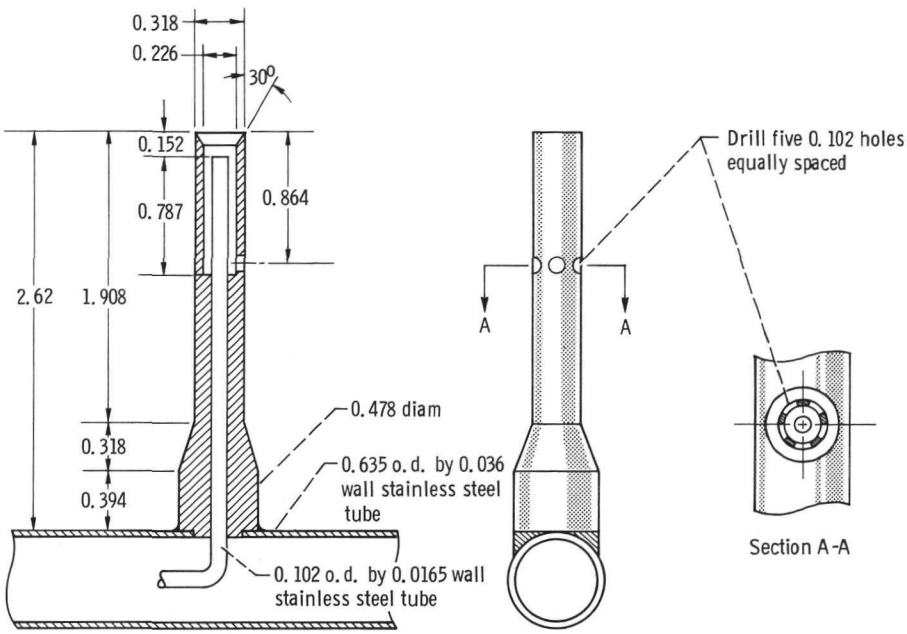

(c) Steady-state total pressure probe. (All linear dimensions are in cm.)

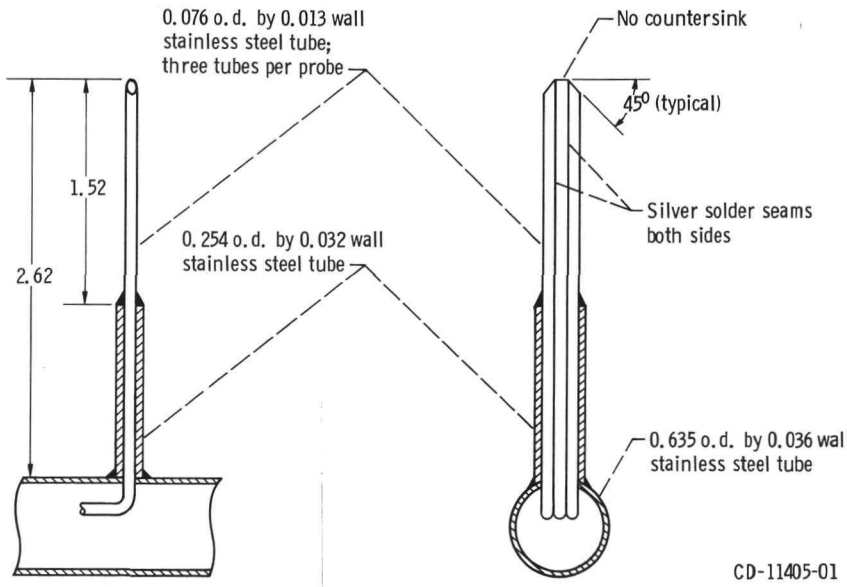

(d) Steady-state flow angularity probe. (All linear dimensions are in cm.)

Figure 5. - Continued.

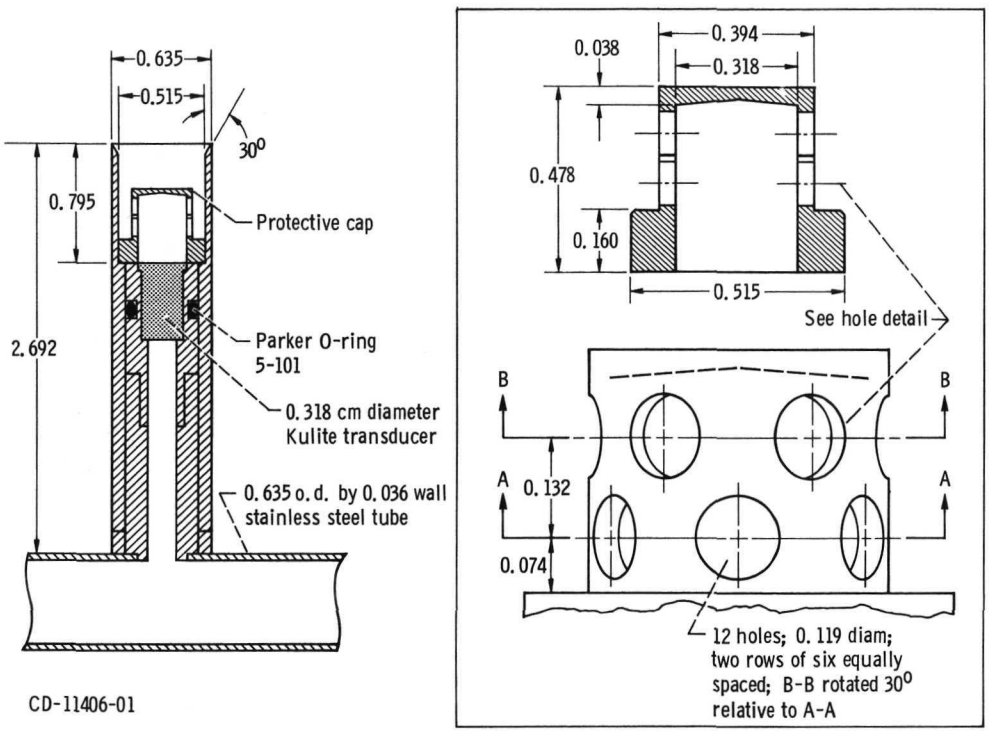

(e) Dynamic total-pressure probe. (All linear dimensions are in cm.)

Figure 5. - Concluded.

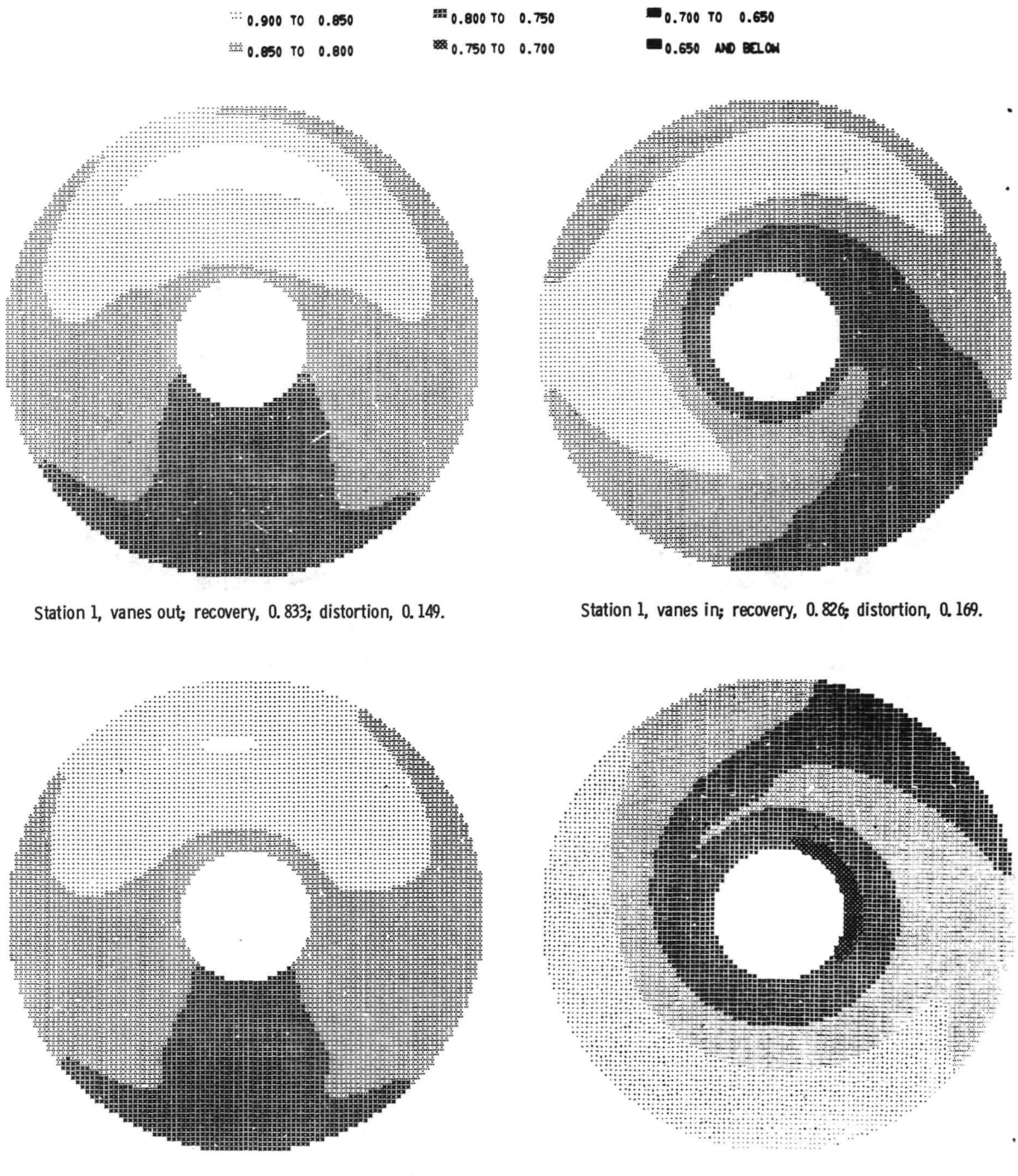

Station 1, vanes out; recovery, 0.833; distortion, 0.149.

Station 1, vanes in; recovery, 0.826; distortion, 0.169.

Station 3, vanes out; recovery, 0.835; distortion, 0.122.

Station 3, vanes in; recovery, 0.822; distortion, 0.176.

(a) Corrected weight flow (minimum), 16.45 kilograms per second.

Figure 6. - Variation of total-pressure profiles with and without swirl vanes for circumferential distortion pattern. Angle of attack, 4.7°; free-stream Mach number, 2.58.

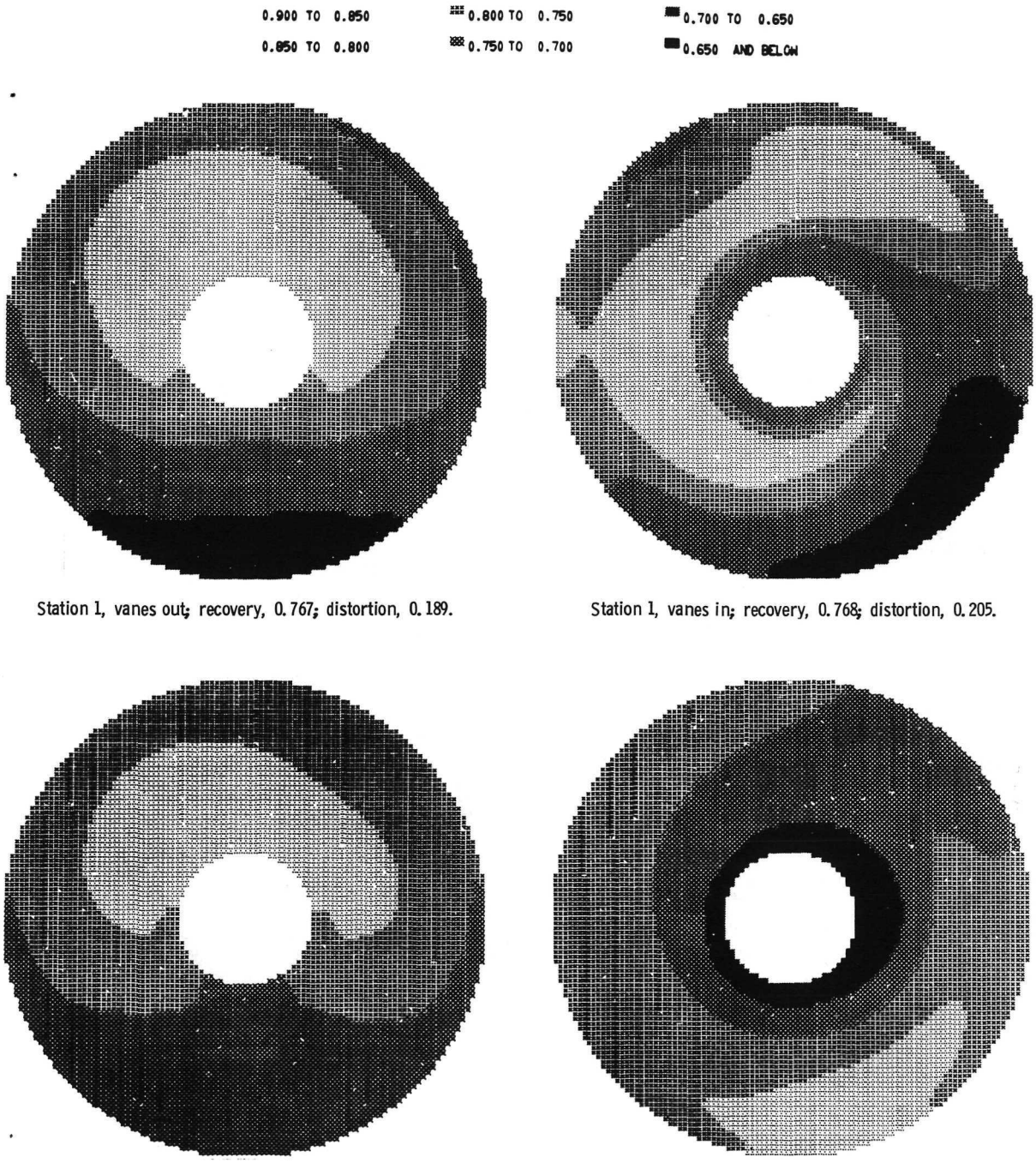

Station 1, vanes out; recovery, 0.767; distortion, 0.189.

Station 1, vanes in; recovery, 0.768; distortion, 0.205.

Station 3, vanes out; recovery, 0.768; distortion, 0.156.

Station 3, vanes in; recovery, 0.756; distortion, 0.257.

(b) Corrected weight flow (supercritical), 17.55 kilograms per second.

Figure 6. - Concluded.

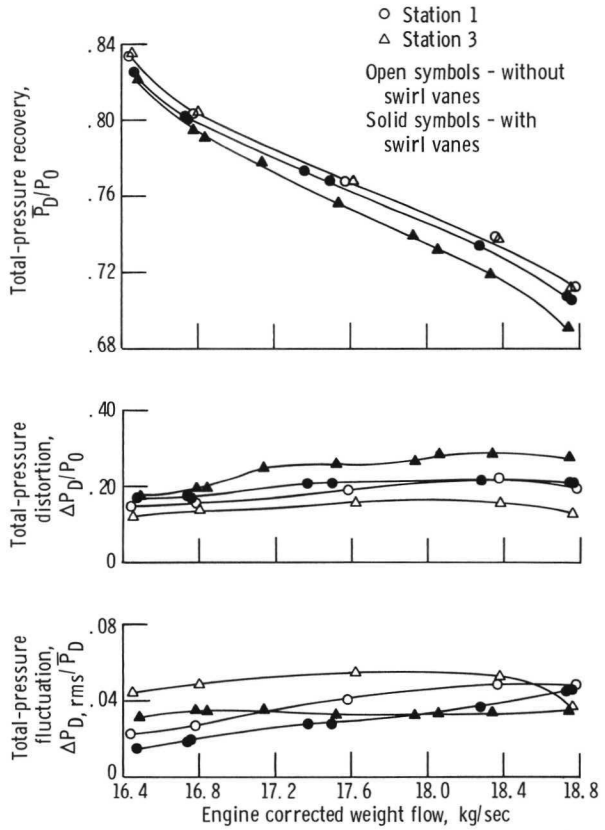

Figure 7. - Variation of diffuser flow properties with and without swirl vanes for circumferential distortion pattern. Angle of attack, 4.7°; free-stream Mach number, 2.58.

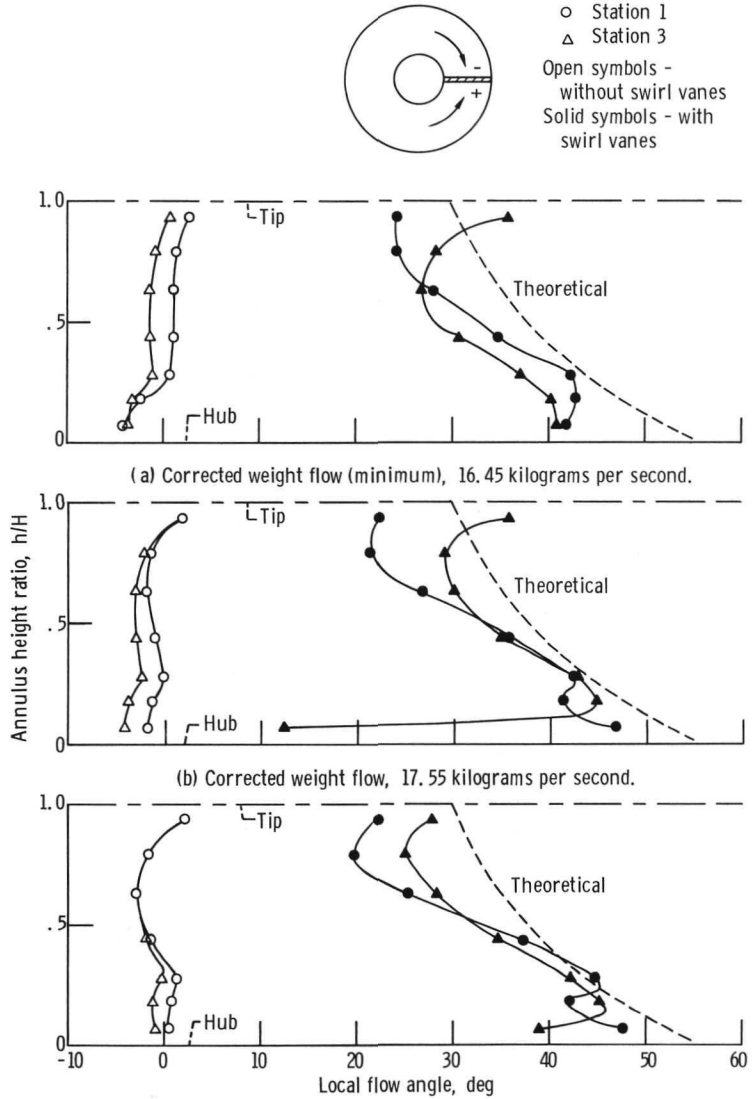

(a) Corrected weight flow (minimum), 16.45 kilograms per second.

(b) Corrected weight flow, 17.55 kilograms per second.

(c) Corrected weight flow, 18.33 kilograms per second.

Figure 8. - Variation of local flow angle at 90° duct position with and without swirl vanes for circumferential distortion pattern. Angle of attack, 4.7°; free-stream Mach number, 2.58.

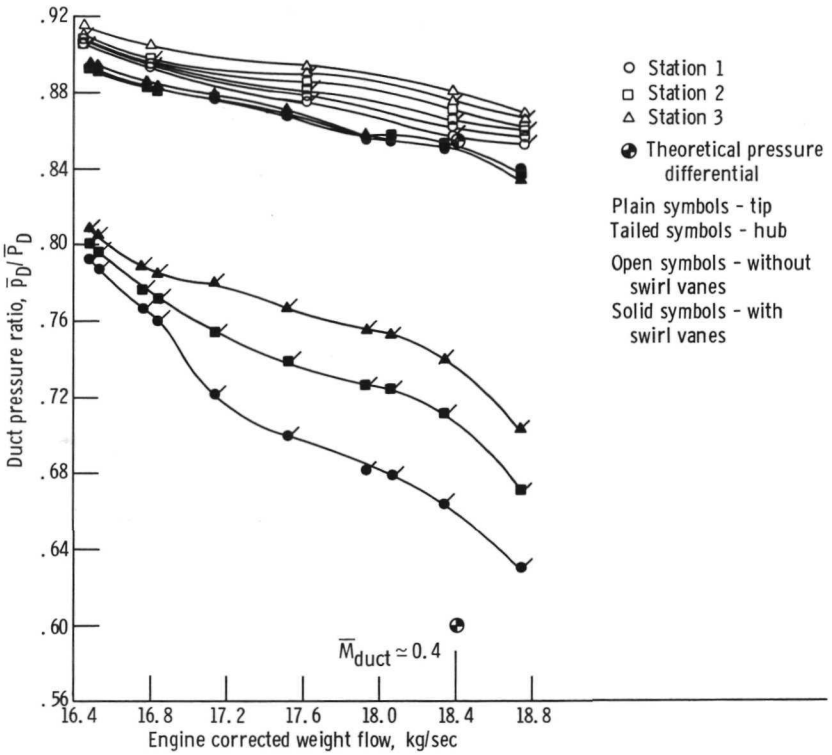

Figure 9. - Variation of duct wall static pressure with and without swirl vanes. Circumferential distortion pattern; angle of attack, 4.7^0; free-stream Mach number, 2.58.

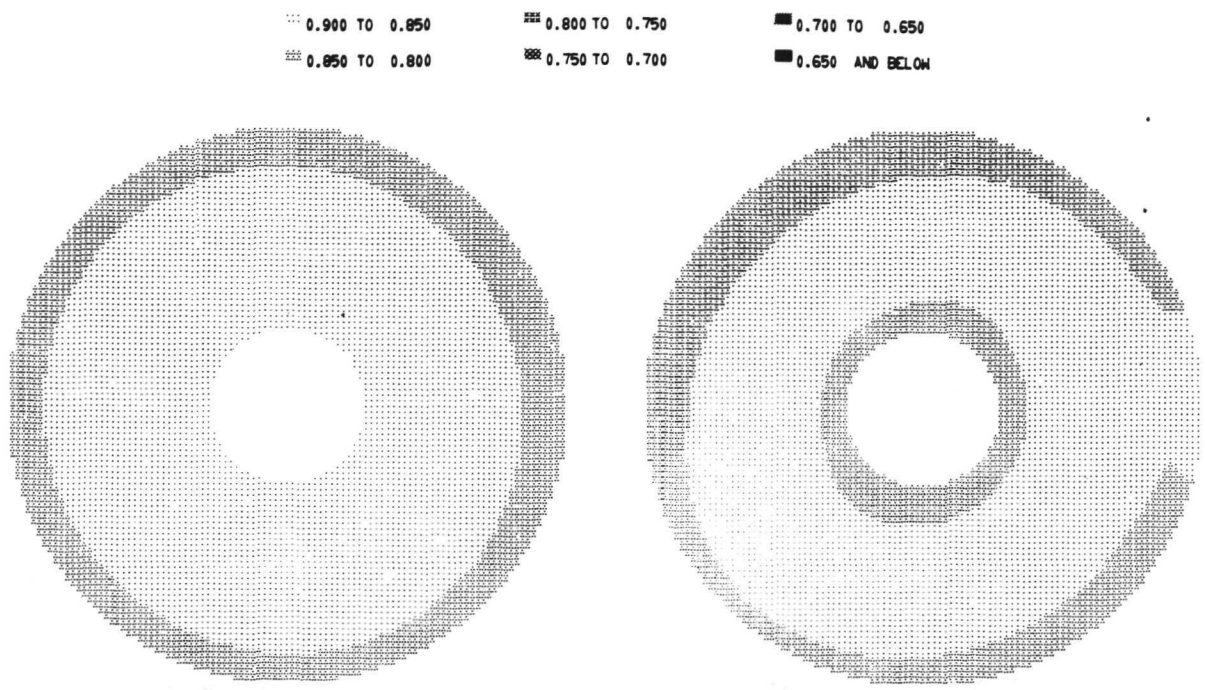

Station 1, vanes out; recovery, 0.863; distortion, 0.069.

Station 1, vanes in; recovery, 0.859; distortion, 0.063.

Station 3, vanes out; recovery, 0.858; distortion, 0.045.

Station 3, vanes in; recovery, 0.848; distortion, 0.047.

(a) Corrected weight flow (minimum), 16.35 kilograms per second.

Figure 10. - Variation of total-pressure profiles with and without swirl vanes for tip-radial distortion pattern. Angle of attack, 0^{o}; free-stream Mach number, 2.58.

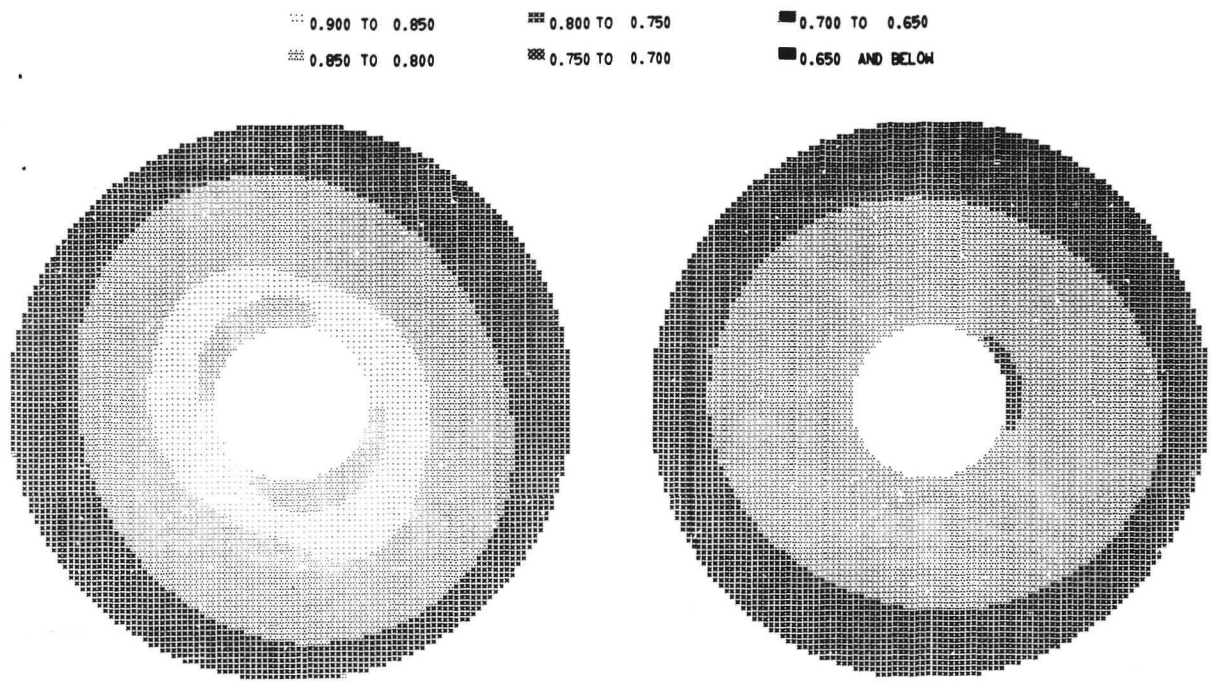

Station 1, vanes out; recovery, 0.814; distortion; 0.116.

Station 1, vanes in; recovery, 0.807; distortion, 0.098.

Station 3, vanes out; recovery, 0.813; distortion, 0.077.

Station 3, vanes in; recovery, 0.799; distortion, 0.104.

(b) Corrected weight flow (supercritical), 17.30 kilograms per second.

Figure 10. - Concluded.

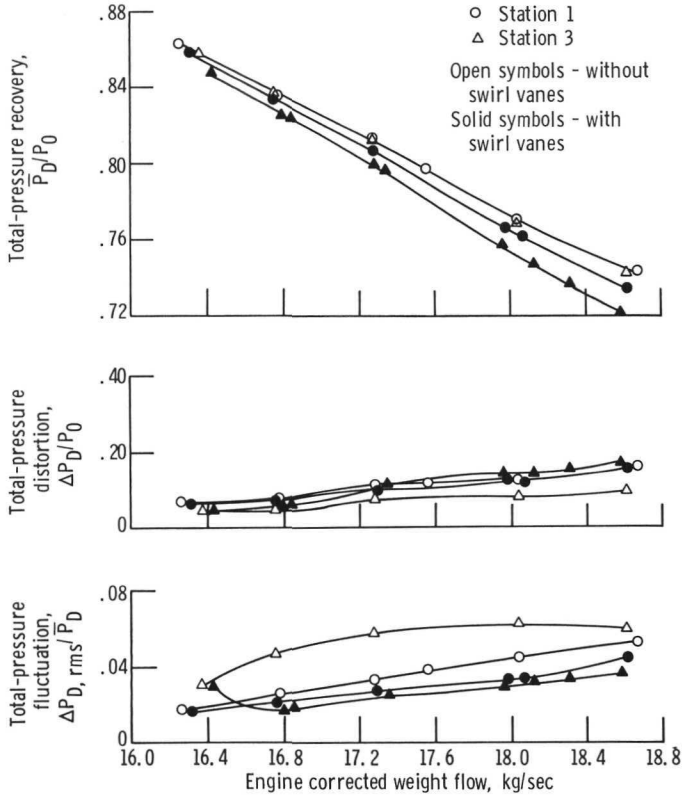

Figure 11. - Variation of diffuser flow properties with and without swirl vanes for tip-radial distortion pattern. Angle of attack, 0^0; free-stream Mach number, 2.58.

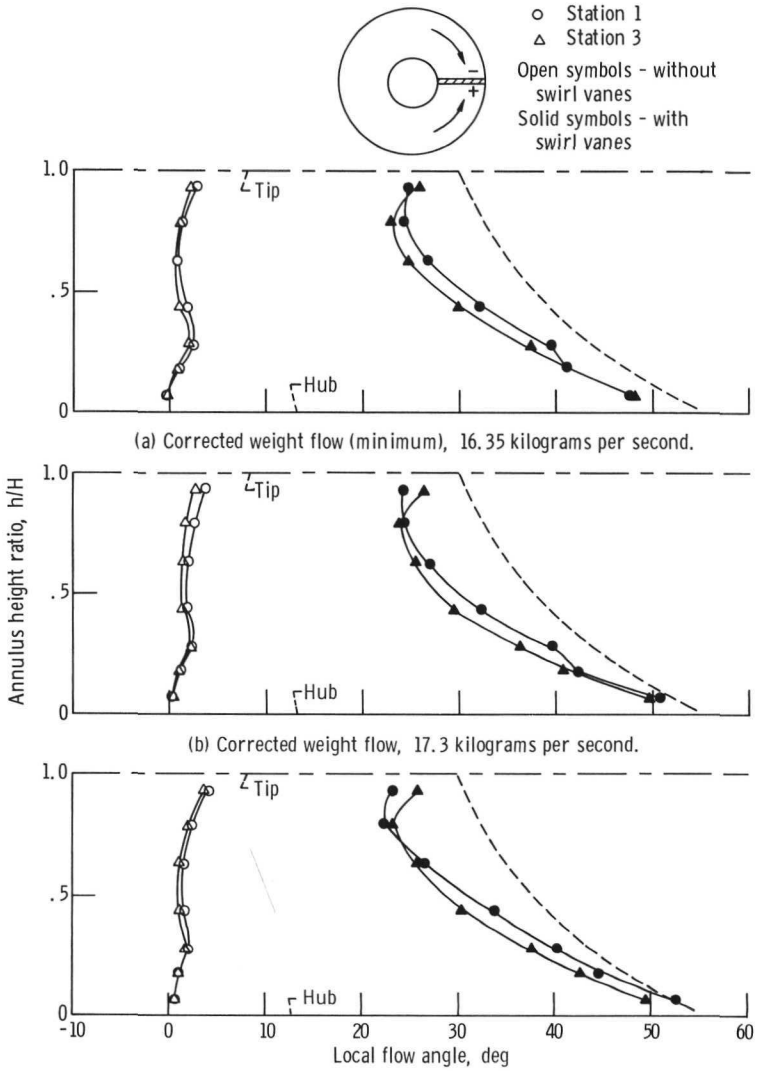

(a) Corrected weight flow (minimum), 16.35 kilograms per second.

(b) Corrected weight flow, 17.3 kilograms per second.

(c) Corrected weight flow, 18.6 kilograms per second.

Figure 12. - Variation of local flow angle at 90^0 duct position with and without swirl vanes for tip-radial distortion pattern. Angle of attack, 0^0; free-stream Mach number, 2.58.

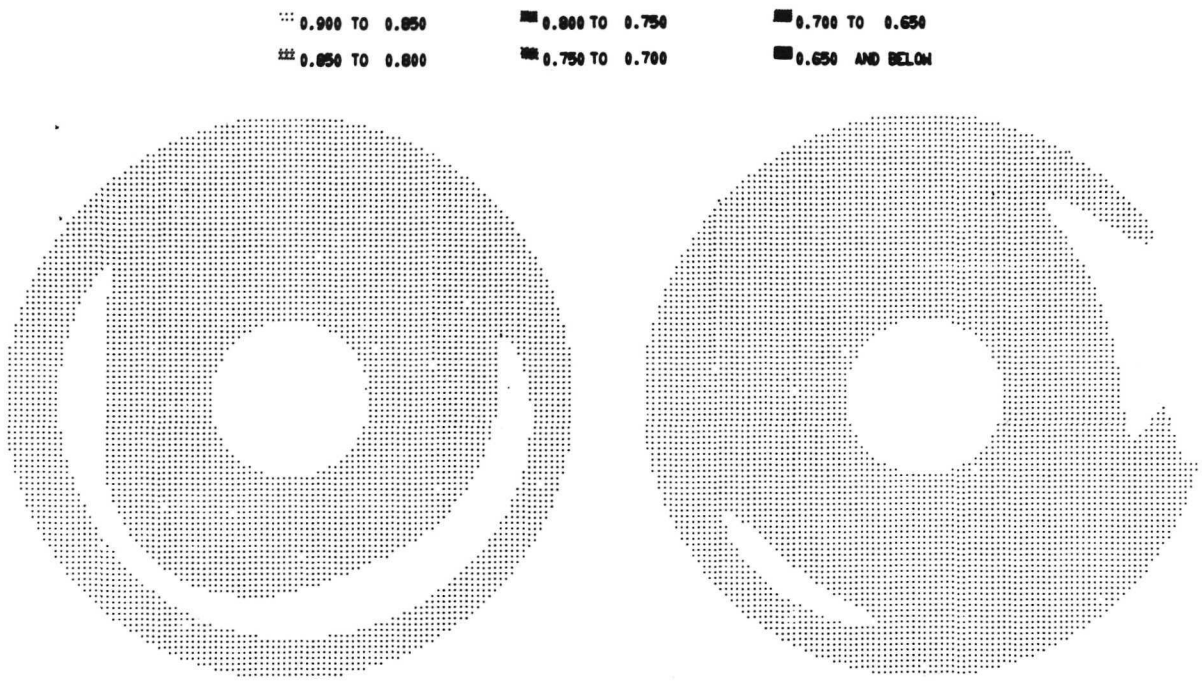

Station 1, vanes out; recovery, 0.889; distortion, 0.043.

Station 1, vanes in; recovery, 0.886; distortion, 0.051.

Station 3, vanes out; recovery, 0.887; distortion, 0.033.

Station 3, vanes in; recovery, 0.883; distortion, 0.043.

(a) Corrected weight flow (minimum); 15.15 kilograms per second.

Figure 13. - Variation of total-pressure profiles with and without swirl vanes for relatively uniform flow. Angle of attack, 0^{o}; free-stream Mach number, 2.58.

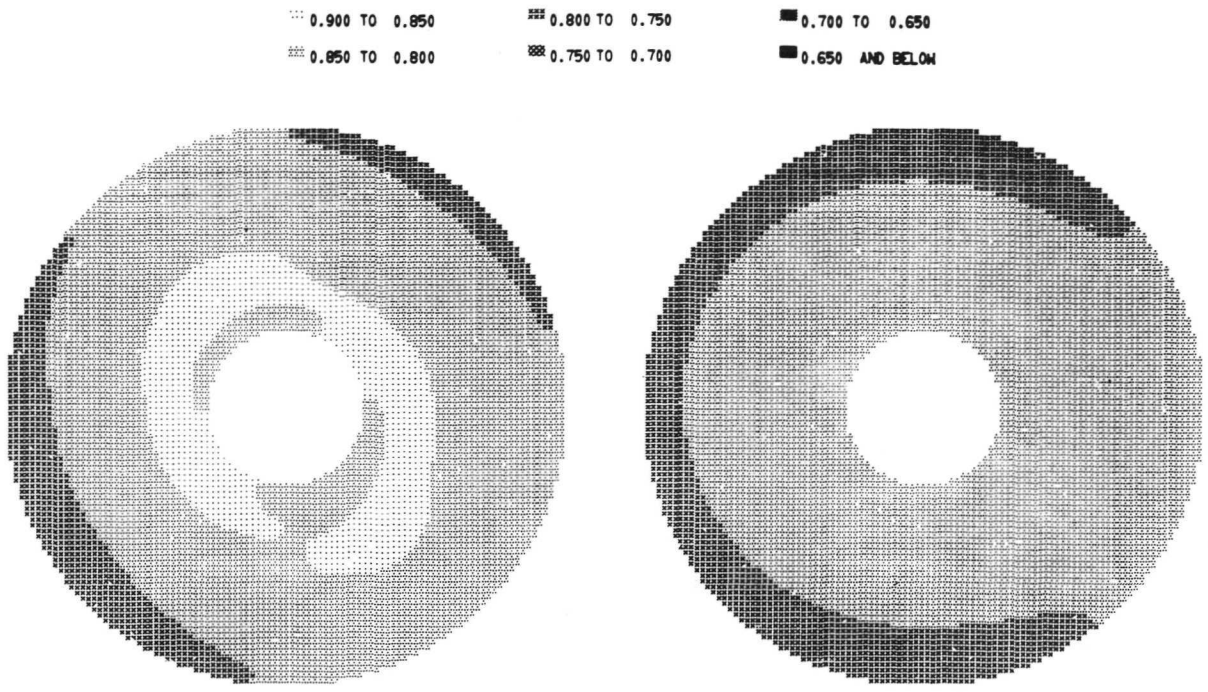

Station 1, vanes out; recovery, 0.825; distortion, 0.089.

Station 1, vanes in; recovery, 0.818; distortion, 0.075.

Station 3, vanes out; recovery, 0.820; distortion, 0.059.

Station 3, vanes in; recovery, 0.807; distortion, 0.097.

(b) Corrected weight flow (supercritical); 16.35 kilograms per second.

Figure 13. - Concluded.

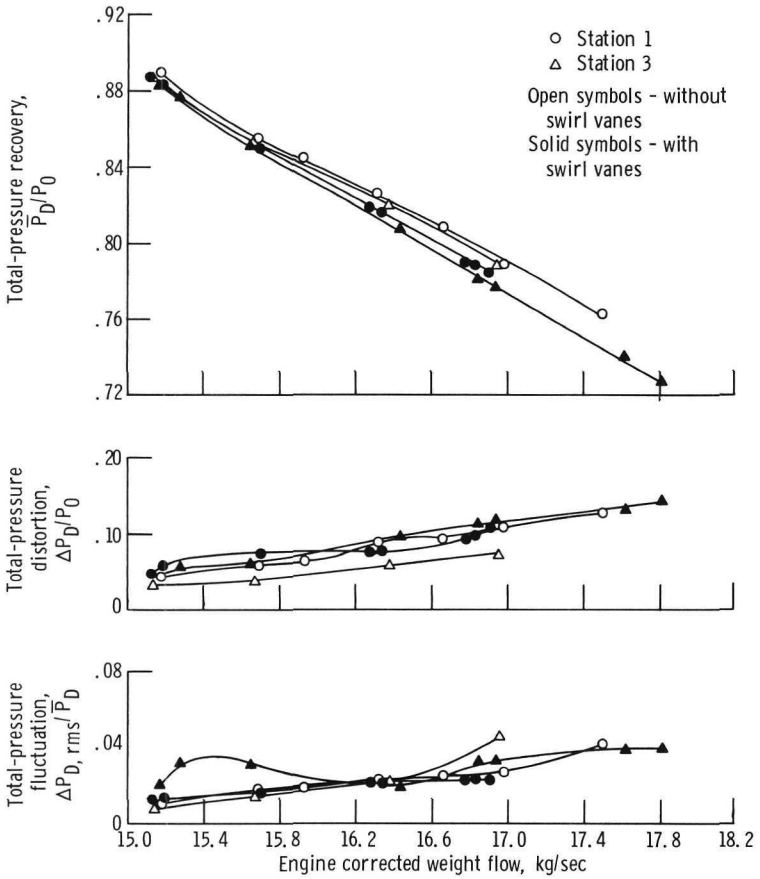

Figure 14. - Variation of diffuser flow properties with and without swirl vanes for relatively uniform flow. Angle of attack, 0^0; free stream Mach number, 2.58.

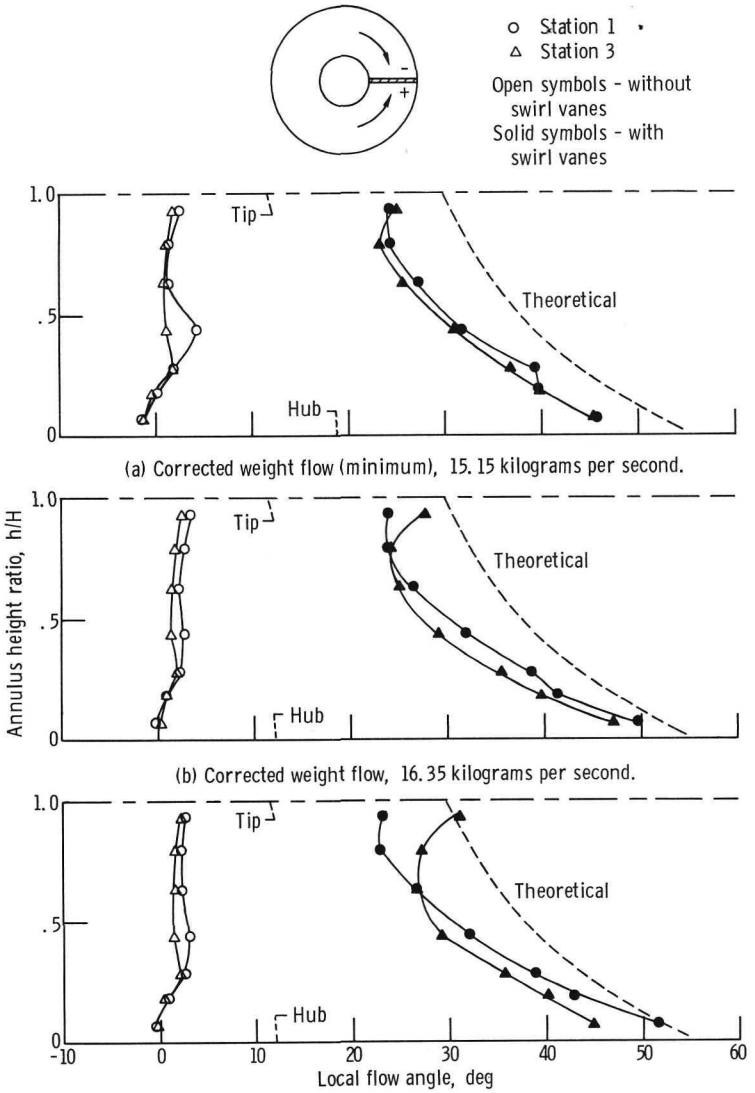

(a) Corrected weight flow (minimum), 15.15 kilograms per second.

(b) Corrected weight flow, 16.35 kilograms per second.

(c) Corrected weight flow, 16.95 kilograms per second.

Figure 15. - Variation of local flow angle at 90^0 duct position with and without swirl vanes for relatively uniform flow. Angle of attack, 0^0; free-stream Mach number 2.58.

"The aeronautical and space activities of the United States shall be conducted so as to contribute . . . to the expansion of human knowledge of phenomena in the atmosphere and space. The Administration shall provide for the widest practicable and appropriate dissemination of information concerning its activities and the results thereof."

—NATIONAL AERONAUTICS AND SPACE ACT OF 1958

NASA SCIENTIFIC AND TECHNICAL PUBLICATIONS

TECHNICAL REPORTS: Scientific and technical information considered important, complete, and a lasting contribution to existing knowledge.

TECHNICAL NOTES: Information less broad in scope but nevertheless of importance as a contribution to existing knowledge.

TECHNICAL MEMORANDUMS: Information receiving limited distribution because of preliminary data, security classification, or other reasons. Also includes conference proceedings with either limited or unlimited distribution.

CONTRACTOR REPORTS: Scientific and technical information generated under a NASA contract or grant and considered an important contribution to existing knowledge.

TECHNICAL TRANSLATIONS: Information published in a foreign language considered to merit NASA distribution in English.

SPECIAL PUBLICATIONS: Information derived from or of value to NASA activities. Publications include final reports of major projects, monographs, data compilations, handbooks, sourcebooks, and special bibliographies.

TECHNOLOGY UTILIZATION PUBLICATIONS: Information on technology used by NASA that may be of particular interest in commercial and other non-aerospace applications. Publications include Tech Briefs, Technology Utilization Reports and Technology Surveys.

Details on the availability of these publications may be obtained from:

SCIENTIFIC AND TECHNICAL INFORMATION OFFICE

NATIONAL AERONAUTICS AND SPACE ADMINISTRATION

Washington, D.C. 20546